Materials Letters 216 (2018) 123–126

Contents lists available at ScienceDirect

Materials Letters

journal homepage: www.elsevier.com/locate/mlblue

Redox deposition of birnessite MnO_2 on ZIF-8 derived porous carbon at room temperature for supercapacitor electrodes

Haibo Sun, Huazhi Gu, Lixing Zhang, Yao Chen *

The State Key Laboratory of Refractories and Metallurgy, Wuhan University of Science and Technology, Wuhan 430081, Hubei, China

ARTICLE INFO

Article history:
Received 11 October 2017
Received in revised form 17 December 2017
Accepted 2 January 2018
Available online 3 January 2018

Keywords:
Carbon materials
Nanocomposites

ABSTRACT

The C/MnO_2 composites were prepared by redox reaction between $KMnO_4$ and the porous carbon derived from sonicated ZIF-8 at room temperature. The C/MnO_2 composite has a specific capacitance of 159 F g^{-1}. The specific capacitance of MnO_2 in the composite is beyond 193 F g^{-1}.

1. Introduction

Over the past few years, supercapacitors with higher power and longer lifetime than secondary batteries have attracted significant attention [1–6]. The main electrode materials of the supercapacitors are carbons, transition metal oxides, and conducting polymers. Carbon based supercapacitors relying on electrical double layer mechanism have higher rate and longer lifetime, while pseudocapacitors based on Faradic reactions of metal oxides or conducting polymers possess higher capacitance [7–9]. Therefore, a hybrid material strategy which combines the advantages of carbon and pseudocapacitive materials can provide synergistic performance for supercapacitors.

MnO_2 is considered to be one of the most attractive pseudocapacitive materials for supercapacitors due to its natural abundance, low cost and environmental benignity [10,11]. In order to overcome the drawback of MnO_2, various carbon materials, such as acetylene black [12], activated carbon [13], carbon nanotubes [14] and graphene [15], have been selected to incorporate into MnO_2. One conventional method to prepare C/MnO_2 composites is to produce MnO_2 with its precursors in the presence of carbon, in which carbon does not participate the reaction. The homogeneity of MnO_2 on carbon depends on the dispersity of carbon in solution. Another method is to etch carbon using Mn^{7+} at high temperature, which ensures the combination of carbon and MnO_2 at the beginning of the reaction [16]. Additionally, it is found that Mn^{7+} can etch acid treated carbon nanotubes at room temperature based on a microelectrochemical cell mechanism, leading to more homogeneous MnO_2 coating initiated by defects from the carbon nanotubes [17].

Recently, metal organic frameworks, especially including ZIF-8, have been exploited as templates/precursors to prepare porous carbons through thermal conversion [18–20]. Further activation of ZIF-8 derived porous carbon can tune its porous structure [21]. In the study, we report the room temperature synthesis of the C/MnO_2 composites by reacting sonicated ZIF-8 derived carbon or its activated product with $KMnO_4$. The C/MnO_2 composite using sonicated ZIF-8 derived carbon shows a specific capacitance of 159 F g^{-1} at 1 A g^{-1}.

2. Experimental

A 250 mL methanolic solution of $Zn(NO_3)_2{\cdot}6H_2O$ (3.718 g) was added into a 250 mL methanolic solution of 2-methylimidazole (1.026 g) and triethylamine (1.634 g), sonicating for 30 min to produce turbid suspension. The turbid suspension was aged for 4 h and then centrifuged to give a white solid, which was washed with methanol and then dried at 80 °C for 4 h to afford sonicated ZIF-8. The sonicated ZIF-8 was kept at 800 °C for 5 h in a furnace under an Ar flow. The resultant material was washed several times with HCl solution (5 vol% in water) and water and dried at 80 °C for 12 h to afford sonicated ZIF-8 derived carbon, denoted as SZC. Further, the SZC sample was activated by KOH at 800 °C for 1 h under Ar, washed with water and dried to give the activated SZC, denoted as ASZC.

0.016 g SZC or ASZC was added to the aqueous solution of 0.04 g $KMnO_4$, stirring under room temperature until the purple color

---

* Corresponding author.
E-mail address: y.chen@wust.edu.cn (Y. Chen).

https://doi.org/10.1016/j.matlet.2018.01.009
0167-577X/

disappeared. The generated composite suspension was filtered, washed, and dired. The products are denoted as SZC/MnO_2 or ASZC/MnO_2.

X-ray diffraction (XRD) patterns were collected by an X'pert Pro MPD diffractometer with Cu K_α radiation. The morphologies and energy-dispersive X-ray spectroscopy (EDS) mapping analyses of the samples were examined by a field emission scanning electron microscope (FESEM, Philips, nanoSEM400) and a transmission electron microscope (FEI TF20). The pore size and volume distribution of the carbon samples were estimated from the nitrogen adsorption/desorption isotherms at 77 K (ASAP 2020) by applying the density function theory.

The electrochemical properties were investigated under a three-electrode configuration. The working electrodes were fabricated by mixing the samples with 15 wt% acetylene black and 5 wt% poly(vinylidene fluoride) in N-methyl-2-pyrrolidone. A platinum sheet and a standard calomel electrode (SCE) were applied as the counter and reference electrodes, respectively. 1 M Na_2SO_4 was used as electrolyte. The cyclic voltammetry (CV) and galvanostatic charge-discharge (GCD) tests were conducted on a CHI660E electrochemical workstation (Shanghai CH Instrument Company, China).

3. Results and discussion

The N_2 adsorption-desorption isotherms and pore distribution curves of SZC and ASZC derived from ZIF-8 and their composites of SZC/MnO_2 and ASZC/MnO_2 are shown in Fig. 1a and b. SZC has a BET specific surface area of 597 $m^2\ g^{-1}$ and a pore volume of 0.42 $cm^3\ g^{-1}$ with both micropores of 0.5–2 nm and mesopores centered at 10 nm. After KOH activation, ASZC exhibits an obviously increased BET specific surface area of 908 $m^2\ g^{-1}$ and a pore volume of 0.62 $cm^3\ g^{-1}$, having a similar pore distribution with those for SZC. Besides, SZC/MnO_2 has the lowest BET specific surface area of 73 $m^2\ g^{-1}$ and a pore volume of 0.15 $cm^3\ g^{-1}$, developing hierarchical porous structure with micropore of 1.3 nm and mesopores centered at 20 nm. ASZC/MnO_2 features a relative large BET specific surface area of 403 $m^2\ g^{-1}$ and a pore volume of 0.26 $cm^3\ g^{-1}$ without big mesopores.

The XRD analysis of SZC/MnO_2 and ASZC/MnO_2 in Fig. 1c confirms the presence of birnessite-type MnO_2 (JCPDS 42-1317). The CHN elemental analysis results reveal that the contents of the remaining C in the SZC/MnO_2 and ASZC/MnO_2 samples are 22.8 and 22.4 wt%, respectively, suggesting that a complete conversion of $KMnO_4$ to MnO_2 occurred in both reactions for SZC and ASZC. It is worth noting that the reaction time is apparently shorter for ASZC, suggesting that more defects catalyze the microelectrochemical deposition of MnO_2.

Fig. 2a–d panels show the SEM images of SZC/MnO_2 and ASZC/MnO_2. It can be observed that rod-like MnO_2 with diameter of 10–30 nm and length of 80–150 nm densely grows on the surface of carbon for both samples. Similar morphology is observed for ASZC/MnO_2. The corresponding EDS mapping images of both samples exhibit the homogeneous MnO_2 distributions on carbon (Fig. S1). Fig. 2e and f panels show TEM images of SZC/MnO_2. It can be seen that MnO_2 homogeneously deposited on activated carbon is consisting of numbers of nanosheets, which indicative of laminated birnessite-type MnO_2.

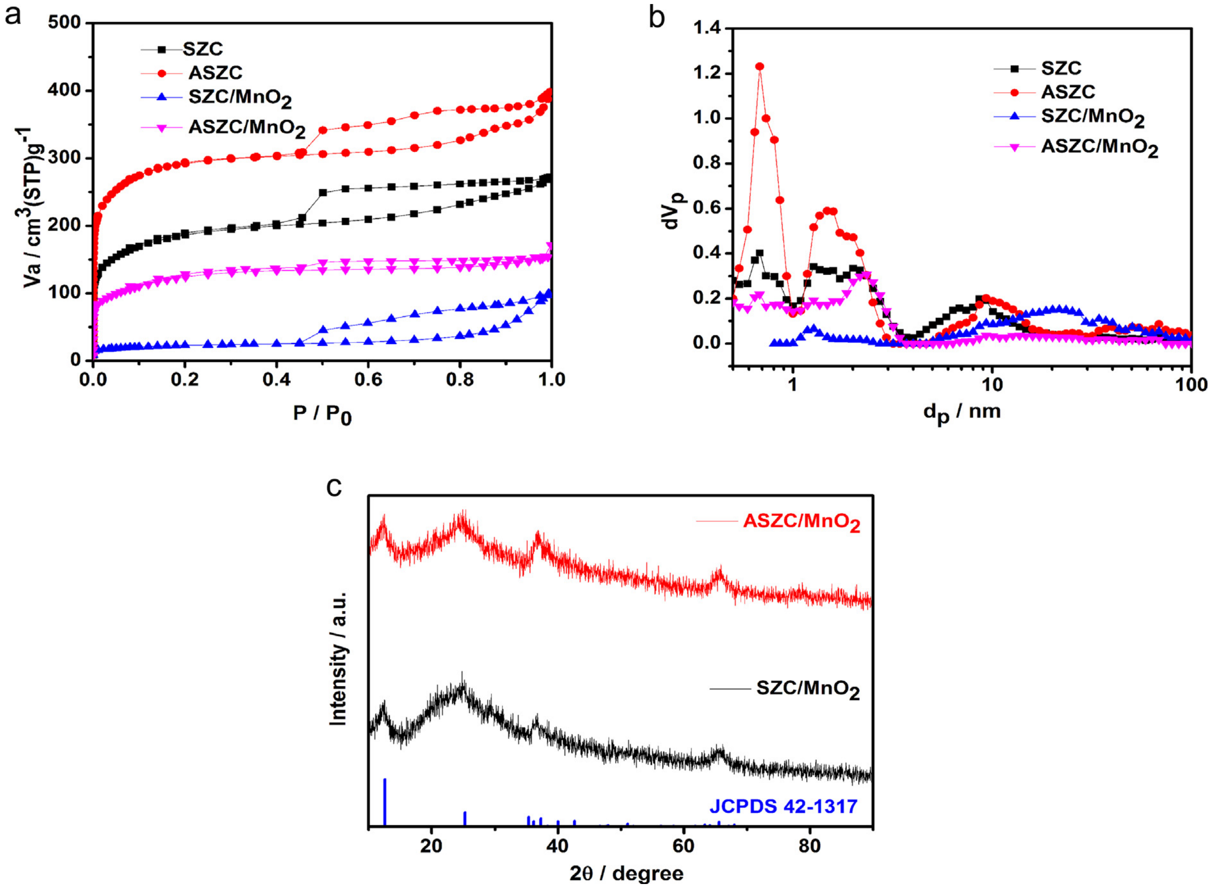

Fig. 1. (a) N_2 adsorption-desorption isotherms and (b) the corresponding pore size distribution curves of SZC, ASZC, SZC/MnO_2 and ASZC/MnO_2. (c) XRD patterns of SZC/MnO_2, ASZC/MnO_2 and JCPDS 42-1317.